Dynamic Strength of Molecular Adhesion Bonds

Evan Evans and Ken Ritchie
Departments of Physics and Pathology, University of British Columbia, Vancouver, British Columbia V6T 1Z1 Canada

ABSTRACT In biology, molecular linkages at, within, and beneath cell interfaces arise mainly from weak noncovalent interactions. These bonds will fail under any level of pulling force if held for sufficient time. Thus, when tested with ultrasensitive force probes, we expect cohesive material strength and strength of adhesion at interfaces to be time- and loading rate-dependent properties. To examine what can be learned from measurements of bond strength, we have extended Kramers' theory for reaction kinetics in liquids to bond dissociation under force and tested the predictions by smart Monte Carlo (Brownian dynamics) simulations of bond rupture. By definition, bond strength is the force that produces the most frequent failure in repeated tests of breakage, i.e., the peak in the distribution of rupture forces. As verified by the simulations, theory shows that bond strength progresses through three dynamic regimes of loading rate. First, bond strength emerges at a critical rate of loading (≥ 0) at which spontaneous dissociation is just frequent enough to keep the distribution peak at zero force. In the slow-loading regime immediately above the critical rate, strength grows as a weak power of loading rate and reflects initial coupling of force to the bonding potential. At higher rates, there is crossover to a fast regime in which strength continues to increase as the logarithm of the loading rate over many decades independent of the type of attraction. Finally, at ultrafast loading rates approaching the domain of molecular dynamics simulations, the bonding potential is quickly overwhelmed by the rapidly increasing force, so that only naked frictional drag on the structure remains to retard separation. Hence, to expose the energy landscape that governs bond strength, molecular adhesion forces must be examined over an enormous span of time scales. However, a significant gap exists between the time domain of force measurements in the laboratory and the extremely fast scale of molecular motions. Using results from a simulation of biotin-avidin bonds (Izrailev, S., S. Stepaniants, M. Balsera, Y. Oono, and K. Schulten. 1997. Molecular dynamics study of unbinding of the avidin-biotin complex. *Biophys. J.*, this issue), we describe how Brownian dynamics can help bridge the gap between molecular dynamics and probe tests.

INTRODUCTION

Held together by noncovalent chemical bonds, we might expect that much of cell structure would dissociate within a modest period if placed in a very dilute environment. However, when sealed in an isolated chamber on a microscope stage, the structure of a single cell persists for a very long time—beyond the limit of the viewer's patience. By comparison, application of mechanical stresses can quickly rupture and render the structure. Under external force, the energetic state of a chemical bond continues to drop as the constituents separate. Conceptually, this leads to an ultimate state comparable to infinite dilution with no likelihood of rebinding. Dissociation under force represents far from equilibrium kinetics, and we can neglect the on rate of bond association from distant regions beyond the domain of attraction. Thus, kinetic traps govern the strength of molecular attachments under external force. In contrast to equilibrium binding affinities, rupture strengths for weak biochemical bonds are not constants but instead depend on the rate of force application and duration of loading.

Received for publication 22 August 1996 and in final form 23 January 1997.

Address reprint requests to Dr. Evan A. Evans, Department of Pathology, University of British Columbia, 6224 Agricultural Rd., Vancouver, BC V6T 1Z1, Canada. Tel.: 604-822-7103; Fax: 604-822-7635; E-mail: evans@physics.ubc.ca.

0006-3495/97/04/1541/15 $2.00

An increased rate of bond dissociation under external force was first emphasized by Bell (1978) using a phenomenological model for the off rate, which is an extension of transition state theory for reactions in gases introduced by Eyring and others (see the outstanding review by Hanggi et al., 1990). In the model of Bell (1978), the off rate, ν, is the product of a natural vibration frequency, ω_o, of the bond in vacuum and the quasi-equilibrium likelihood of reaching the transition state with an energy barrier, E_b, discounted by mechanical energy $f \cdot x_\beta$ (force $\times$ displacement) to give $\nu \sim \omega_o \exp[-(E_b - f \cdot x_\beta)/k_B T]$. The applied force, f, is assumed to act directly along a reaction coordinate, x, to reach x_β at the transition state; $k_B T$ sets the thermal energy scale. Hence, the off rate should rise exponentially with force, i.e., $\nu \approx \nu_o \exp(f/f_\beta)$, above a characteristic level, $f_\beta = k_B T/x_\beta$. The importance of Bell's insight was to expose the significant role of mechanical force in biological chemistry, but all features of the energy landscape are lumped into one parameter—a length, x_β. Recognizing this limitation, we introduced a different model in which the off rate was assumed to follow a power law at low forces in the vicinity of f_β, i.e., $\nu \sim \nu_o (f/f_\beta)^b$, to capture variations in rupture behavior from ductile ($b \leq 1$) to brittle ($b > 1$) failure (Evans et al., 1991). Of more fundamental significance, we showed that peaks observed in histograms of bond strength arise because forces applied to the bonds increase progressively in time (Evans et al., 1994; Evans, 1995).

In this article, we critically examine the physics that underlies bond strength. Extending the Brownian dynamics theory of Kramers (1940; Hanggi et al., 1990) for kinetics in liquids to force-driven dissociation of bonds, we demonstrate that the off rate follows a general form given by $\nu = \nu_o\, g(f)\, \exp[\Delta E_b(f)/k_BT]$, where the functions $g(f)$ and $\Delta E_b(f)$ depend on deformation of the energy landscape by external force and the spatial variation of frictional interactions between molecules. In the context of laboratory experiments, the theory predicts three regimes of bond strength with distinct dependencies on the rate of loading. With the advent of ultrasensitive mechanical techniques, the strength of molecular attachments can now be tested with nanoscale resolution (e.g., atomic force microscope (AFM); Hoh et al., 1992; Radmacher et al., 1992; Lee et al., 1994; Florin et al., 1994; Moy et al., 1994; Williams et al., 1996; biomembrane force probe (BFP); Evans et al., 1994, 1995; and optical tweezers (OT); Ashkin et al., 1990; Kuo and Sheetz, 1993). Along with other methods (e.g., Tees et al., 1993; Alon et al., 1995), the techniques have been used to probe many types of attachments to cell surfaces and solid substrates. However, to date, no approach has been controlled sufficiently well to discriminate between kinetic models for unbonding or to measure the dependence of bond strength on loading rate. On the other hand, Grubmuller et al. (1996) and Izrailev et al. (1997) have demonstrated new schemes to examine bond breakage under external force in molecular dynamics (MD) simulations of biotin-streptavidin and biotin-avidin bonds. At the slowest pulling or loading rates ($\sim 10^{12}$ piconewtons (pN)/s), the rupture forces derived from simulations are within a factor of 2 of the forces measured in AFM experiments at rates of 10^4 pN/s. Although satisfying in this respect, the molecular simulations remain widely separated in time (eight orders of magnitude or more in loading rate) from the physical realm of mechanical probe experiments, and comparison of the results with laboratory tests can be illusive. Therefore, with a smart Monte Carlo (SMC) algorithm capable of spanning the gap in loading rate, we have also performed Brownian dynamics simulations of bond breakage to test the off rate kinetics predicted by the theory of Kramers (1940) critically and to examine how experimental measurements can be connected with MD simulations.

THEORY

Brownian dynamics theory of unbinding under constant force in liquid environments

In condensed liquids, the thermal impulses that drive dissociation are dissipated rapidly by viscous coupling to the environment. Hence, the prefactor ν_o in the off rate is not governed solely by a vibration frequency ω_o of the bond; viscous friction ultimately limits the kinetic process. This important feature of kinetics in liquid environments was first brought out in a famous article by Kramers (1940; Hanggi et al., 1990). Kramers analyzed the thermal noise-driven escape of a particle over a potential barrier using the Fokker-Planck approximation for Brownian motion through a phase space. In such a microcanonical approach, the unbinding kinetics are idealized as a steady flux of probability density along a preferential path from a deep energy minimum outward over a barrier via a saddle point in the energy surface. There can be many such paths, and the paths can map out complex trajectories in phase space. However, application of an external pulling force acts to collimate the reaction path, which we define by the scalar coordinate x. Assumed to be bounded by steeply rising energy in other directions, a conceptual illustration of the energy landscape, $E(x)$, along this coordinate is sketched in Fig. 1 *A*. As shown in Fig. 1, *B* and *C*, the external force contributes a disjoining potential, $-f \cdot x$, which tilts the energy landscape and modifies the shape, magnitude, and location of the energy barrier, E_b, at the transition state ($x = x_{ts}$), which is defined by the maximum of the combined energies. We will use Kramers' approach to predict the rate of dissociation from the bound state over these deformed landscapes. [To simplify terms, energies will be normalized by k_BT (i.e., $E \equiv E/k_BT$ and $f \cdot x \equiv f \cdot x/k_BT$) and distances by a microscopic length, x_a (i.e., $x \equiv x/x_a$) defined by the choice of the bonding potential. Thus, forces are scaled by $f_a = k_BT/x_a$ (i.e., $f \equiv f/f_a$).]

In the following analysis, dissociation under force is assumed to be slowed sufficiently by viscous damping so that there are many thermal impulses per escape, and the external force is assumed stationary over the time scale of these excitations. Because velocity distributions remain nearly Maxwellian, dissociation can be modeled by spatial diffusion of thermalized states over the barrier. The transport of states out of the confining potential obeys the Smoluchowski equation (Kramers, 1940; Hanggi et al., 1990), which in one-dimension (1-D) is represented by the flux J (#/time),

$$J(x) \approx D\{(f - \partial E/\partial x)\rho - \partial \rho/\partial x\} \qquad (1)$$

Here, $\rho(x)$ is the local density (#/length) of states along the reaction coordinate with the obvious normalization $\int \rho \cdot dx = 1$; D ($\equiv D/k_BT$) is the local mobility or diffusivity of states limited by viscous friction γ (i.e., $D = k_BT/\gamma$). Assumed to be stationary (J = constant), Eq. 1 can be integrated between bound and free states ($a \rightarrow f$) to give the general result,

$$J \approx -\{\rho \cdot \exp(E - f \cdot x)\}_{a \rightarrow f} \Big/ \int_{a \rightarrow f} dx \cdot \exp(E - f \cdot x)/D(x) \qquad (2)$$

Appearing inside the integral (denominator), the viscous impedance to diffusion may vary with separation along the reaction coordinate. In general, two categories of viscous damping can be envisioned. The first is an intrinsic friction in which energy is dissipated directly in fast relaxation processes internal to the molecular structure and coupled to

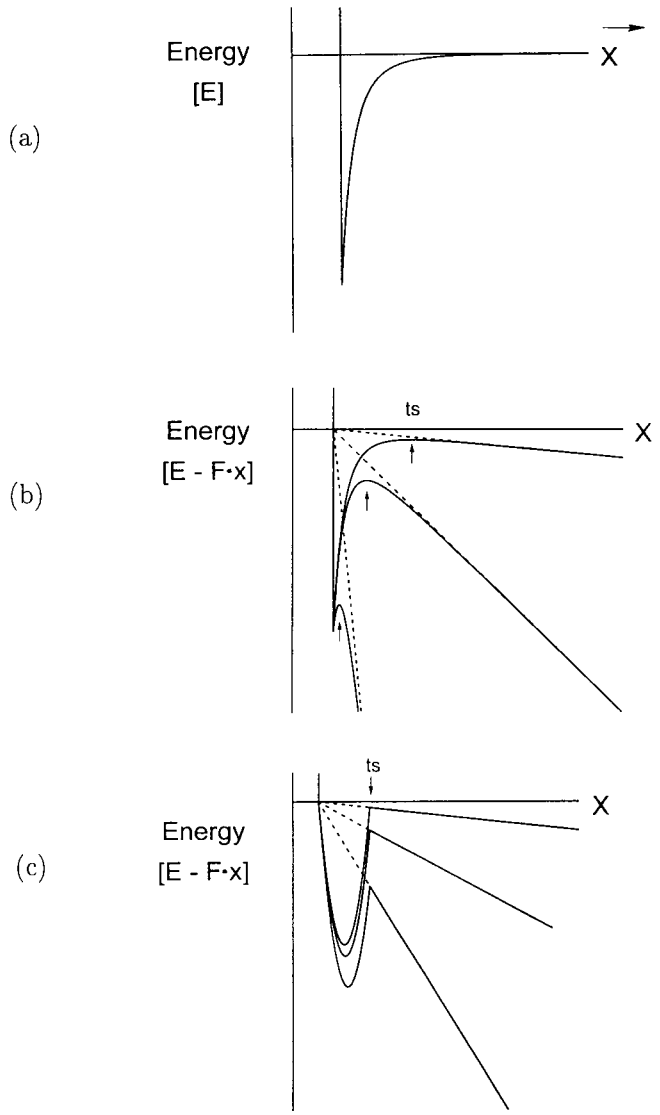

FIGURE 1 (*A*) Conceptual view of the energy landscape along a reaction pathway in unbonding. Idealized as distance, the x axis defines a generalized reaction coordinate in configuration phase space. The bound state is labeled a, and the free state f is assumed to lie well beyond the range of the potential. (*B*) Tilt and deformation of the energy landscape caused by application of force to a bond defined by an inverse power law attraction. The mechanical potential $-f \cdot x$ creates a well-defined transition state located at the maximum in the combined energy, $E(x) - f \cdot x$. The transition state moves inward, and the barrier height E_b is reduced progressively as force increases. (*C*) Tilt and deformation of the energy landscape caused by application of force to a bond defined by a deep harmonic well. The mechanical potential leads to a sharp cusp at the transition state instead of the broadly curved maximum shown in (*B*). For the steeply rising potential, the transition state remains fixed, and the minimum is shifted outward as force increases.

the liquid environment through large conformational fluctuations on slower time scales. The other is extrinsic friction in which energy is dissipated by rigid body translations and rotations of the molecules in the liquid, i.e., hydrodynamic damping. Although both types of friction may depend on location, we will assume that friction can be modeled by a constant, γ_o, plus a hydrodynamic interaction, γ_H, which is consistent with the results and conclusions of Ansari et al. (1992, 1994). For unbonding in three-dimensions (3-D), a mobility tensor must be constructed to model hydrodynamic impedance to longitudinal, transverse, and rotational movements of the structures in the fluid environment (Batchelor, 1976). However, under a pulling force, the important quantity is the principal value of the tensor along the direction of force, which, to first order, increases with separation in the range less than the Stokes radii of the molecular components. The hydrodynamic interaction γ_H diminishes approximately with distance along the reaction coordinate. Hence, we will examine the following representative models for mobility: 1) $D_o \approx$ constant, dominated by intrinsic friction; 2) $D \approx D_o x/\delta_o$ on the scale of the potential, dominated by extrinsic hydrodynamic interaction. The minimum separation δ_o is assumed to be maintained by short-wavelength excitations (fluctuations) local to the binding pocket.

Under force, the free state at $x_f \rightarrow \infty$ becomes a perfectly adsorbing boundary at which the density of states, $\rho_f \approx 0$, and Eq. 2 lead to the following form for the off rate ν:

$$\nu \approx (D/l_a l_b)\exp(-E_b + \Delta E_b) \tag{3}$$

The diffusive nature of the unbonding kinetics is expressed in the prefactor $D/l_a l_b$, which represents the frequency of attempts to escape. The exponential $\exp(-E_b + \Delta E_b)$ is the quasi-thermal likelihood of reaching the top of the energy barrier at the transition state x_{ts}. The reduction ΔE_b in the height of the energy barrier results from tilt of the energy landscape by the mechanical potential $(-f \cdot x)$, as shown in Fig. 1, *B* and *C*. The density of states ρ_a local to the minimum at x_a defines the length $l_a = 1/\rho_a$. Because most of the states lie deep in the energy well, the length, l_a, is effectively the departure from the minimum for a $k_B T$ increase in energy. Usually, a harmonic approximation local to the energy minimum is used to represent l_a,

$$l_a \approx \int dx \cdot \exp(-\kappa_a x^2/2) = (2\pi/\kappa_a)^{1/2}$$

where κ_a is the elastic stiffness (curvature) of the harmonic well. Given an effective mass m, the characteristic mechanical resonance frequency $\omega_o/2\pi$ of the bond would be $(\kappa_a/m)^{1/2}$. The length l_b is the statistically weighted width of the barrier defined by the integral in the denominator of Eq. 2. For constant damping ($D = D_o$), the barrier width is expressed by,

$$l_b = \int_{a \rightarrow f} dx \cdot \exp[\Delta(E - f \cdot x)_{ts}] \tag{4}$$

where $\Delta(E - f \cdot x)_{ts} = E(x) - E_{ts} - f \cdot (x - x_{ts})$ is maximum at the transition state x_{ts}. On the other hand, for strong hydrodynamic interaction ($D \approx D_o x/\delta_o$, with $\delta_o \approx l_a$), the decrease in damping with separation contributes a weak

logarithmic term to the argument of the statistical weight inside the integral,

$$l_b \approx \int_{a\to f} dx \cdot \exp\{\Delta[E - f\cdot x - \ln(x)]_{ts}\} \qquad (5)$$

Hence, the transition state, defined at the maximum of $[E - f\cdot x - \ln(x)]$, is displaced from x_{ts}. Note for centrosymmetric potentials in d dimensions and in the absence of force, the barrier width integral has the form $\sim \int dx \cdot \exp(E)/[x^{d-1}D(x)]$. Hence, a linear dependence of mobility on separation has an effect similar to increasing the spatial dimension in Kramers' theory.

Isolating the force-dependent factors in Eq. 3, we obtain a generic expression for the off rate under force given by,

$$\nu = \nu_o g(f)\exp[\Delta E_b(f)] \qquad (6)$$

where $g(f) \equiv 1/l_b$. The prefactor ν_o contains the Arrhenius dependence on barrier energy scaled by a characteristic time constant, t_D, for diffusive escape,

$$\nu_o = (1/t_D)\exp(-E_b)$$

where $t_D \equiv l_a/D$ $(=l_a x_a/D)$. The dimensionless functions $g(f)$ and $\Delta E_b(f)$ determine the force-driven amplification of the kinetics.

Given simple types of bonding potentials, the location of the transition state and reduction ΔE_b in barrier height are readily found by algebraic manipulation. The principal task is to determine the barrier width, l_b defined by Eq. 4 or 5. If the energy falls off sufficiently fast on either side of the barrier, then asymptotic methods (saddle point integration) can be used to evaluate the integral. However, the barrier width diverges, and Kramers' stationary flux treatment breaks down in dimensions ≤ 2 when the energy monotonically approaches a plateaux at zero force (cf. Fig. 1 *A*). In such pathological situations, three-dimensional characteristics of the kinetics and long-range diffusion are usually taken into account to determine the off rate (see Hanggi et al., 1990). On the other hand, a pulling force always leads to a well-defined transition state amenable to simple analytical treatment. From a purely phenomenological point of view then, spontaneous dissociation of an isolated bond (at infinite dilution) can be postulated to arise from a transient repulsion that decays after unbonding. Conceptually, the putative repulsion stems from the nonequilibrium initial condition that molecular states beyond the region of strong attraction must be suppressed at times $t \leq 0$, and, in the context of Kramers' theory, a broad transition state remains at zero force. We examine this postulate in the simulations described later. To make specific predictions that can be tested by simulations, we will analyze two types of attractive potentials, an inverse power law and a deep harmonic well, which deform quite differently under force.

Dissociation under force from an inverse power law attraction

As illustrated in Fig. 1 *B*, we begin with the attractive potential $E \sim -A/x^n$ (e.g., $n = 6$ for a van der Waals interaction). The depth of the potential is fixed by an infinite repulsive wall at the microscopic length $x_a = (A/E_b)^{1/n}$, which sets the location x_m $(= 1)$ of the minimum and defines $A = E_b$. Derived from $\partial(E - f\cdot x)/\partial x = 0$ for constant damping, the transition state is located at $x_{ts} = (f_\infty/f)^{1/n+1}$, where f_∞ is the bare (zero temperature) strength of the bond defined by the maximum attraction nE_b at x_a $(= 1)$. Reduction in height of the energy barrier at x_{ts} increases with force according to,

$$\Delta E_b = E_b[(n + 1)(f/f_\infty)^{n/n+1} - n(f/f_\infty)]$$

The transition state and minimum vanish with the barrier when $f \geq f_\infty$. Following our normalization convention, forces are scaled by $f_a = k_B T/x_a$. The sensitivity level for force in laboratory measurements is set by the force f_β needed to lower the energy barrier by $k_B T$, which depends weakly on the binding potential; i.e., $f_\beta \approx n/\{(n + 1)[(n + 1)E_b]^{1/n} - (n + 1)\}$. When $f < E_b$, reduction in the energy barrier is well approximated by $\Delta E_b \approx (f/f_\beta)^{n/(n+1)} \sim (f/f_\beta)$.

To evaluate the barrier width l_b in Eq. 4, the combined energy is expanded to quadratic order near the transition state as follows:

$$\Delta(E - f\cdot x)_{ts} \approx -\kappa_{ts}(x - x_{ts})^2/2$$
$$\approx -[(n + 1)f/x_{ts}](x - x_{ts})^2/2$$

The elastic stiffness (curvature) is essentially proportional to the force; i.e., $\kappa_{ts} = (\partial^2 E/\partial x^2)_{ts} = (n + 1)f/x_{ts}$. Using the expansion, the barrier width is approximated by,

$$l_b \approx \int_{ts} dx \cdot \exp[-\kappa_{ts}(x - x_{ts})^2/2] \approx (2\pi/\kappa_{ts})^{1/2}$$

which yields,

$$l_b \approx [2\pi/(n + 1)nE_b]^{1/2}(f_\infty/f)^{(n+2)/2(n+1)}$$

Therefore, the off rate is predicted to increase with force according to,

$$\nu = \nu_o g(f)\exp\{E_b[(n + 1)(f/f_\infty)^{n/n+1} - n(f/f_\infty)]\} \qquad (7)$$

with $g(f) = 1/l_b$. When $f < E_b$, the off rate closely follows $\nu \sim (f/f_\beta)^{1/2}\exp(f/f_\beta)$ for large n. Cutoff by a steep repulsion at x_a, the length scale l_a in the prefactor ν_o is estimated by the location of an energy level of $k_B T$ above the minimum; i.e., $l_a \approx 1/(nE_b)$.

Turning now to strong hydrodynamic interaction in which molecular mobilities increase with separation on the scale of the potential, all of the properties of the transition state change in subtle but important ways. The transition state is specified by solution to the equation, $x_{ts}^{n'} = nE_b -$

$x_{ts'}^{(n+1)} f$, which now has an upper bound of $(nE_b)^{1/n}$ as $f \to 0$. Over the full range of force, a useful approximation for the position is given by $x_{ts'} \approx (nE_b)^{1/n}/\{1 + [(nE_b)^{1/n} - 1](f/f_{\infty'})^{n/2(n+1)}\}$. The transition state and minimum vanish at a force, $f_{\infty'} = nE_b - 1$, slightly below the zero temperature bond strength. Best expressed in terms of $x_{ts'}$, the reduction in the energy barrier is found to be,

$$\Delta E_b = f \cdot [(n+1)x_{ts'}/n - 1] + \ln(x_{ts'}) + 1/n$$

which approaches the expected limit E_b at the force $f_{\infty'}$. Recognizing where linear and logarithmic terms become significant, integration of Eq. 5 yields the following approximation for the barrier width:

$$l_b \approx (2\pi/n)^{1/2} x_{ts'}/(f \cdot x_{ts'} + n) + \exp[-(f \cdot x_{ts'})^2/(f \cdot x_{ts'} + n)] \cdot \ln(1 + 1/f \cdot x_{ts'})$$

Therefore, the off rate is predicted to increase with force according to,

$$\nu = \nu_o g(f) \exp\{f \cdot [(n+1)x_{ts'}/n - 1] + \ln(x_{ts'}) + 1/n\} \quad (8)$$

where again $g(f) = 1/l_b$. When $1 < f < f_\infty$, the off rate approaches the result given in Eq. 7 for constant molecular damping. Strong hydrodynamic interaction mainly affects the increase in off rate under small forces, because the barrier width diverges weakly as the logarithm of force instead of $\sim 1/f^{1/2}$.

Dissociation under force from a deep harmonic well

If the potential rises more steeply from the bound state than an inverse power law, the mechanical disjoining potential can lead to a quite different transition state with a sharp discontinuous cusp, as illustrated in Fig. 1 *C*. To examine this case, we model the potential as a deep harmonic well with an elastic stiffness, $\kappa_a = (2E_b)$, where the distance scale $x_a \equiv (2E_b/\kappa_a)^{1/2}$. The transition state is fixed at $x_{ts} = 2$. However, as given by $x_m = 1 + (f/f_\infty)$, the minimum shifts progressively outward and, along with the transition state, vanishes when the force reaches the bare strength of the bond $f_\infty = 2E_b$. The thermal force scale is $f_\beta \approx 1 + 1/4E_b$. Relative to the displaced minimum, the reduction in height of the energy barrier increases with force according to,

$$\Delta E_b \approx 2E_b[(f/f_\infty) - (f/f_\infty)^2/2]$$

which for $f < E_b$ closely follows $\Delta E_b \approx (f/f_\beta)$. Because the minimum of the combined potential shifts on application of force, there will be an initial transient in the kinetics at time $t = 0^+$ as the distribution relaxes in the tilted landscape and states begin to permeate the barrier region. The stationary flux assumption in Kramers' theory breaks down during the transient. The characteristic ratio of time scale for the transient to time scale for diffusion past the barrier is $\sim \exp\{-E_b[1 - (f/f_\infty)^2]\}$. The ratio shows that the initial transient can be neglected when the force is below $f/f_\infty \sim 1 - 1/E_b^{1/2}$. In this range, the barrier energy exceeds k_BT, and the rate of dissociation is limited by permeation of states through the barrier. These states have sufficient time to equilibrate in the displaced harmonic well. At the other extreme of high force, the rate of dissociation becomes limited by a transient outflow of states from the initial distribution independent of the small barrier at x_{ts}. For now, we ignore the initial transient and examine the lower range of external force.

In calculating the barrier width, we can treat the molecular friction as constant and neglect hydrodynamic interaction over the scale of the harmonic well except at very small forces. Local to the cusplike transition state, the energy falls off linearly with distance on either side of the barrier so that the integral in Eq. 4 is evaluated in two parts. From x_{ts} inward to the displaced minimum x_m, the integral is represented by the function $I_1(y) = \int_o^y ds \cdot \exp[-(2E_b - f)s + E_b s^2]$, which is on the order of $1/2E_b$ or less, where the argument is defined by $y = 1 - f/2E_b$. Adding the integral from the transition state outward, we obtain the following expression for the barrier width for constant damping:

$$l_b \approx I_1(1 - f/f_\infty) + 1/f$$

(As for inverse power law attraction, the main effect of introducing strong hydrodynamic interaction is to replace $1/f$ by a weak logarithmic divergence in the barrier width as the applied force approaches zero.) Therefore, below $f/f_\infty \sim 1 - 1/E_b^{1/2}$, the off rate is predicted to increase according to,

$$\nu = \nu_o g(f) \exp\{2E_b[(f/f_\infty) - (f/f_\infty)^2/2]\} \quad (9)$$

with $g(f) = 1/l_b$ and the length scale l_a implicit in ν_o approximated by $1/\rho_a \approx (\pi/E_b)^{1/2}$. The off rate closely follows the relation $\nu \sim (f/f_\beta) \exp(f/f_\beta)$.

Ultrafast dissociation under extreme forces

Under very large forces, the extreme tilt of the energy landscape leads to ultrafast kinetics as the most prominent of the energy maxima, E_b^* (located at x_{ts}^*), is overwhelmed by the mechanical potential. Here, details of molecular bonding are important, because the energy contour along the reaction coordinate may be irregular with more than one maximum in energy. Before reaching the ultrafast limit, there can be a cascade of crossovers in which the position x_{ts} of the transition state jumps from one intervening maximum to the next (as we will show later using results from simulations of biotin-avidin by Izrailev et al., 1997). When the most prominent barrier is eliminated, all states are essentially unbound, and the kinetics of dissociation are only transiently retarded by weak topographical features of the highly tilted energy landscape. Naively then, for a single barrier, the off rate should diverge as $f \to f_\infty$ ($\sim \max \nabla E$). However, before this level of force is reached, the rate of

dissociation can become limited by the transient outflow of states from the initial minimum at $t = 0^+$ as approximated by $\nu \sim D \cdot (f - f_{\infty'})$. This is equivalent to the rate of free transport, first diffusion then rapid drift driven by an excess force $(f - f_{\infty'})$, over the scale of the potential as if no potential existed. For a harmonic well, this limit is reached when $f_{\infty'} = f_\infty\ (1 - 1/E_b^{1/2})$. At even higher forces, the distribution of velocities in phase space could begin to distort from a Maxwellian distribution so that the kinetics would deviate from the spatial diffusion limit modeled by the Smoluchowski relation. Such consequences were considered by Kramers 50 years ago and examined in greater detail more recently (Hanggi et al., 1990).

Spontaneous dissociation at zero force

At the other limit at which force goes to zero, the off rates expressed in Eq. 7–9 also go to zero, because the barrier width diverges in one dimension. For the reasons discussed earlier, we hypothesize that a small intrinsic repulsion, f_i, can be introduced to model the crossover to spontaneous dissociation, and that this repulsion weakly augments the action of external force. Thus, the off rate near $f \sim 0$ would increase approximately as a low power of force for constant damping,

$$\nu \sim (f_i/f_\beta + f/f_\beta)^b \tag{10a}$$

with $b \sim 1/2$ given an inverse power law attraction or $b \sim 1$ given a harmonic well. But for strong hydrodynamic interaction, the form of the bonding potential is masked by the logarithmic divergence in the barrier width near $f \sim 0$, and the off rate would approach,

$$\nu \sim 1/\ln[f_\beta/(f_i + f)] \tag{10b}$$

for all potentials. As we will describe in a later section, simulations of bond rupture have been used to test this phenomenological model for spontaneous dissociation. In short, the results show that for both types of bonding potential and strong hydrodynamic interaction in dimensions $\geq$1-D, a level of force can be identified below which the dissociation rate is independent of force. However, with constant damping and inverse power law attraction in one dimension, no crossover could be established in simulations of bond rupture.

Most important at small forces, the reaction path followed in unbonding may be strongly distorted by molecular mechanics and map out a highly curved trajectory in space. Indeed, detachment may involve force-driven switching between several reaction paths in phase space. Although detailed knowledge of the structure is needed to evaluate unbonding trajectories for complex molecules, we can easily imagine qualitative categories of force coupling to the energy landscape. At one extreme, external forces may be leveraged mechanically to assist separation. This would tilt the energy landscape downward at low force and reduce the barrier more than expected. At the other extreme, separation may be sterically hindered in the direction of the applied force so that significant elastic deformation of the structure would be needed to begin unbonding (e.g., curved structures that hook together). The energy landscape would tilt upward under low force and augment the barrier more than expected. (Similar concepts were suggested many years ago by Dembo et al. (1988), in which sterically hindered bonds were labeled as catch bonds and ideal bonds as slip bonds.) At some level of force, the reaction coordinate will line up with the force to produce the idealized linear coupling. Phenomenologically then, the characteristic force, f_β, at which the energy barrier is reduced by k_BT could be altered significantly by molecular mechanics and not related simply to a bond length, x_β; e.g., f_β would be $< k_bT/x_\beta$ for leveraged bonds and $> k_bT/x_\beta$ for hindered bonds. As such, the generic form for the off rate under force can still be represented by $\nu = \nu_o\ g(f)\ \exp[\Delta E_b(f)]$, but $g(f)$ and f_β now reflect the possibility of more complex mechanical couplings to the energy landscape at low force.

Dissociation of bonds under dynamic loads (increasing force)

In the previous section, we derived expressions for kinetics of unbonding under constant applied force. The assumption of stationary force is valid for fast molecular relaxation times but fails to capture the feature that application of force always involves a mechanical transient. Unlike MD simulations, application of force in all mechanical experiments occurs over a time scale much longer than relaxation times for thermal impulses. In force probe techniques, a transducer is usually moved at a constant speed $\Delta x/\Delta t$ relative to a substrate in which the bond is anchored. Therefore, if we neglect deformation of the substrate, the load on the bond increases at a constant rate $\Delta f/\Delta t = k_f\ (\Delta x/\Delta t)$ set by the speed and the transducer stiffness k_f (force/displacement). Given bond strengths on the order of 100 pN, the force ramp would span periods of $> 10^{-3}$ s before bond rupture even with the fast AFM ($\Delta f/\Delta t \sim 10^4$–$10^5$ pN/s). Much longer periods of loading would be needed for more sensitive techniques such as BFP ($\Delta f/\Delta t \sim$ 1–10^3 pN/s) and OT ($\Delta f/\Delta t \sim$ 1–10 pN/s). Clearly, mechanical loading is extremely slow compared with thermal impulses lasting $< 10^{-12}$ s. Hence, the probability of bond survival is no longer a simple exponentially decaying function of time determined by a constant off rate. The likelihood of bond detachment under force represents a first-order kinetic process with a time-dependent rate of dissociation, i.e., $\nu[f(t)]$. Within a small interval of time $(t, t + dt)$, the probability of failure is expressed by,

$$p(t,f) = \nu(f)\exp\left\{-\int_{o\to t} \nu[f(t')]\cdot dt'\right\} \tag{11}$$

where $\exp\{-\int_{o\to t} \nu[f(t')]\cdot dt'\}$ is the likelihood of bond survival to time t (Evans et al., 1991; Evans, 1995). For the

precise history $f = (\Delta f/\Delta t) \cdot t$, force and time are directly related so that force can be viewed as the independent random variable. Introducing the generic form for off rate, the probability density for failure can be expressed as a dimensionless function of force f ($\equiv f/f_a$),

$$p(f) = (1/r_f)g(f)\exp[\Delta E_b(f)] \cdot \exp\left\{ -(1/r_f)\int_{o\to f} g(y)\exp[\Delta E_b(y)]\,dy \right\} \quad (12)$$

parameterized by the dimensionless loading rate $r_f \equiv (\Delta f/\Delta t)/\nu_o f_a$. The statistical distribution of rupture events is the product of an off rate that increases in time and a likelihood of bond survival that decreases with time, which can exhibit a maximum at a specific time (≡force) as illustrated in Fig. 2. As such, bond strength is a dynamic property defined by the force f^* for most frequent failure at the peak of the rupture force distribution. The strength peak represents the most likely period of survival (lifetime) of the bond under a particular rate of loading but is not constant. Instead, bond strength increases with the rate of loading. The location of the peak and characteristic spread of the distribution are obtained from derivatives of the distribution given in Eq. 12. The maximum ($\partial p/\partial f = 0$) in the distribution defines the location of the peak,

$$[\nu/\nu_o]_{f=f^*} = r_f[\partial \ln \nu/\partial f]_{f=f^*} \quad (13)$$

which is solved to find the dependence of strength on loading rate. The curvature $[-(1/p)\partial^2 p/\partial f^2 = 1/\Delta_f^2]$ of the distribution local to the maximum at f^* provides a measure of the spread Δ_f in the distribution given by,

$$1/\Delta_f^2 = [(\partial \ln \nu/\partial f)^2 - (\partial^2 \ln \nu/\partial f^2)]_{f=f^*} \quad (14)$$

Readily determined from the dependence of the distribution peak f^* on the loading rate r_f in Eq. (13), dissociation under a ramp of force and the generic form for off rate lead to three regimes of dynamic strength. These regimes are confirmed by SMC simulations described in the next section.

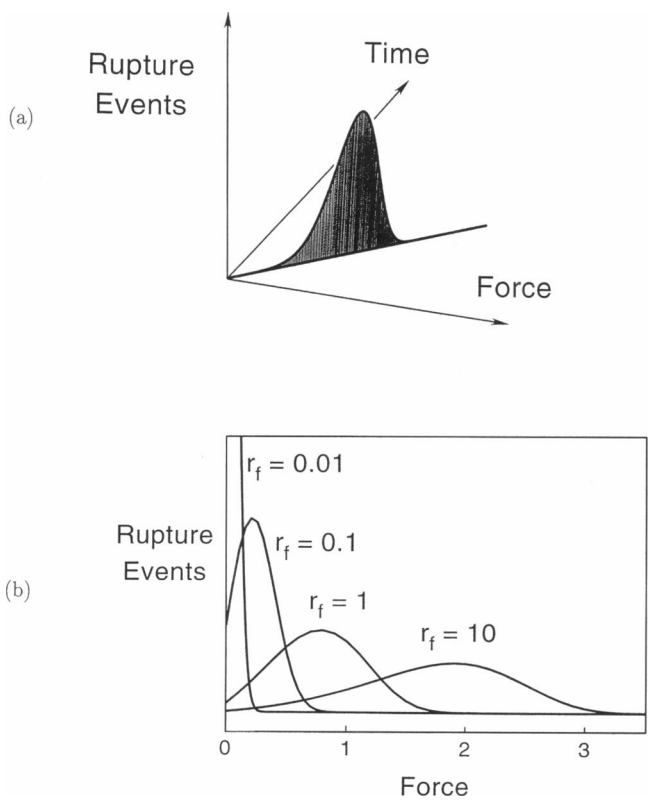

FIGURE 2 (*A*) Illustration of rupture forces predicted for bonds over time and force in mechanical probe tests. Loaded by a ramp of force, the off rate increases steadily, but the likelihood of bond survival decreases simultaneously. Thus, the frequency of failure can reach a maximum at some time equivalent to force; the peak defines the bond strength f^*. (*B*) Plotted versus instantaneous force; rupture force distributions shift with loading rate r_f.

Brownian dynamics simulations of bond breakage under a ramp of force

Simulation of molecular actions in liquids is challenging because there are huge numbers of degrees of freedom. To capture fine details of chemistry, all aspects of atomic structure and interactions must be included, which is the motivation for MD simulations. However, at present, MD computations provide only a nanosecond glimpse of the system, which hinders comparison with experiments that probe molecular assemblies on NMR time scales or longer ($>10^{-6}$ s). At the other extreme, at which atoms are modeled as structureless balls that interact via idealized potentials, Monte Carlo methods can be used to simulate diffusive relaxation of a system toward equilibrium. Here, random displacements of the particles at each time step are accepted or rejected by a Boltzmann energy-weighted criterion (Metropolis et al., 1953). Some years ago, Rossky et al. (1978) introduced a smart version of the Monte Carlo algorithm to simulate overdamped Brownian dynamics in a liquid medium. In this concept, force-driven displacements scaled by particle mobilities are combined with randomly selected diffusive movements to create trial steps at each time. New positions are then accepted with modified Metropolis probabilities based on joint Boltzmann and dynamic transition probabilities. In this way, the system of particles obeys overdamped Langevin dynamics, which can be efficiently explored over many orders of magnitude in time with an arbitrary scale set by the characteristic diffusion time. Using this approach and a Pentium desktop computer, we have simulated many millions of time steps in the course of bond rupture under a ramp of force and explored an eight-order-of-magnitude range in loading rate. The particular simulations were set up: 1) to test the predictions of Kramers' theory for bond dissociation under increasing force, especially at low force in one dimension, in which the theory is nontrivial; and 2) to compare bond rupture in 3 dimensions lations with that in one dimension. In the simulations, a

tensile force was used to separate a spherical test particle from another spherical particle anchored rigidly at a point. As in the theoretical analysis, we compared constant damping with strong hydrodynamic interaction, in which damping decreases inversely with separation at close range. To model Langevin dynamics properly, the dynamic transition probability in the SMC algorithm was modified to include the spatial gradient in diffusivity so that the trial movements Δr for each time step Δt were statistically weighted by both the Boltzmann factor and $\exp\{-[\Delta r - (D \cdot \Delta t)f - \nabla D]^2/(4D \cdot \Delta t)$.

MATERIALS AND METHODS

Before the start of each simulation ($t < 0$), the bond was preequilibrated in the potential at low temperature ($E_b = 80$) to initialize the test particle close to the energy minimum. Then, the temperature was jumped to the desired level ($3 < E_b < 7$) at $t = 0$, and the disjoining force was increased at a preset rate for $t \geq 0$. Bond rupture was identified by the condition that the test particle continued to move well beyond the location of the transition state. During the simulation, every crossing of the transition state was noted. As shown in Fig. 3, the time of final passage of the transition state differed significantly from the time of first passage at slow loading rates with many intervening passages and returns. At faster loading rates, the last passage time approached the first passage time, which then became an equivalent estimator of bond lifetime and strength. Because force increased steadily over the simulation, the value of force at rupture was specified by the time of final crossing of the transition state multiplied by the constant loading rate. Bond strengths were examined at 55 loading rates over an eight-order-of-magnitude range including rates at which loading quickly overwhelmed the bonding potential.

At every loading rate, we performed 200 simulations of bond breakage to provide statistics for the rupture force distribution. Even so, histograms of rupture forces at set loading rates still contained statistical variations, as illustrated by specific examples in Fig. 4. In the upper range of loading rates at which mean rupture forces exceeded f_a ($\equiv 1$), every histogram had an obvious peak. Here, either the theoretical probability distribution (defined by Eq. 12 with the appropriate off rate expression) or a simple Gaussian distribution would give equally good fits to the distribution and to locate the peak (cf. Fig. 4, *C* and *D*). However, in the range of very slow loading rates at which the mean rupture force was below $f \approx 1$, determination of the peak was more elusive, and the location became indistinguishable from zero force given the statistical variations in the histogram (cf. Fig. 4, *A* and *B*). To assay for a peak, it was necessary to analyze the exponential-like decay in rupture events in the histogram. At slow loading rates, the decay parameter (in units of 1/force) multiplied by the loading rate provided an estimator of the mean off rate [$\langle \nu \rangle \sim (1/t) \int_{o \to t} \nu(t') \cdot dt'$]. Labeled as an apparent mean off rate, we used this estimator to test the off rate directly for sensitivity to force and to locate the crossover to spontaneous dissociation from force-driven kinetics. If the off rate was in a range not sensitive to force, then the apparent mean off rate had to be independent of the loading rate and vice versa because of the first-order kinetics defined by the probability density in Eq. 12. Plots of the apparent mean off rates versus loading rate in Fig. 5 demonstrate the crossover behavior. Modeled by Eq. 10a or 10b, definition of the critical rate by this procedure established an empirical assay for an intrinsic repulsion, f_i. Based on the values derived for intrinsic repulsion and the theoretical prescriptions for off rate under force, probability distributions were calculated for the histograms as shown by the curves superposed on the results in Fig. 4.

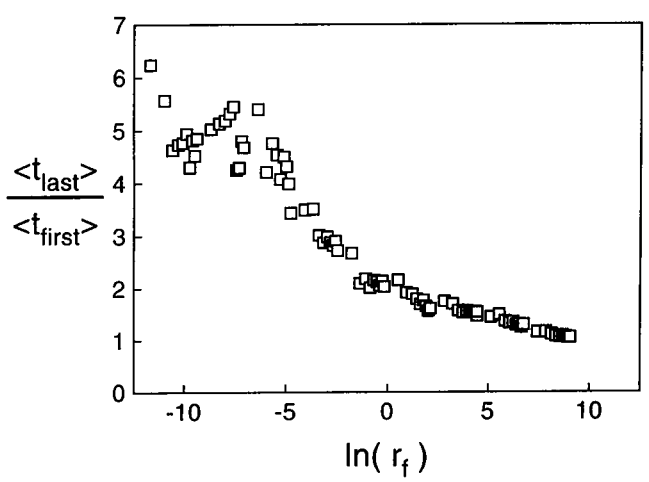

FIGURE 3 Average time of final passage of the transition state divided by the average time of first passage in simulations of bond breakage under constant loading rate. In the lower range of loading rates, many intervening escapes and returns occur in Brownian diffusion before rupture on final passage of the energy barrier. As loading rate increases, the last passage time (t_{last}) approaches the first passage time (t_{first}).

RESULTS

The 1-D simulations of bond breakage were performed for the two types of bonding potential and the friction model described in Theory. (For the inverse power law attraction, exponents in the range of $1 \leq n \leq 6$ were examined, but because the simulations verified the theoretical dependence on this exponent, we only present results for $n = 4$.) To plot the results and predictions on the same scale, loading rates were normalized by the characteristic rate $\nu_o = (1/t_D)\exp(-E_b)$ set by the simulation parameters. The results inFig. 6 from simulations with an inverse power law attraction provide a comparison between models of constant intrinsic damping and a strong hydrodynamic interaction that diminished with separation. In Fig. 7, results from simulations assuming strong hydrodynamic interaction provide a comparison between the deep harmonic well and inverse power law potentials. The theoretical predictions of strength superposed on the simulation results in Figs. 6 and 7 yielded exceptional correlations over the full range of loading rates. In Figs. 6 *A* and 7 *A*, $\log(f^*)$ versus $\log(r_f)$ plots show that strength increased as a weak power of rate under slow loading, which defined the initial regime of strength. In the simulations with strong hydrodynamic interaction, strength emerged at a well-defined critical rate of loading for both bonding potentials. Below the critical rate of loading, no strength was perceived for the bond, because the peak in the distribution of rupture forces stayed at zero force. Listed in the figure legends, the critical rates were used to derive empirical values for the intrinsic repulsion, f_i, postulated in Theory. At the critical rate, the time needed to reach the level of the intrinsic repulsion was comparable to the spontaneous lifetime of the bond, i.e., $f_i/(\Delta f/\Delta t) \sim 1/\nu_{f \to o}$. By comparison, in 1-D simulations with constant damping, strength continued to decrease to miniscule levels as rates were lowered; no critical rate was detected for the loading rates examined. Next, as shown by the plots in Figs. 6 *B* and 7 *B*, strength continued to rise when $r_f > 1$ but now in

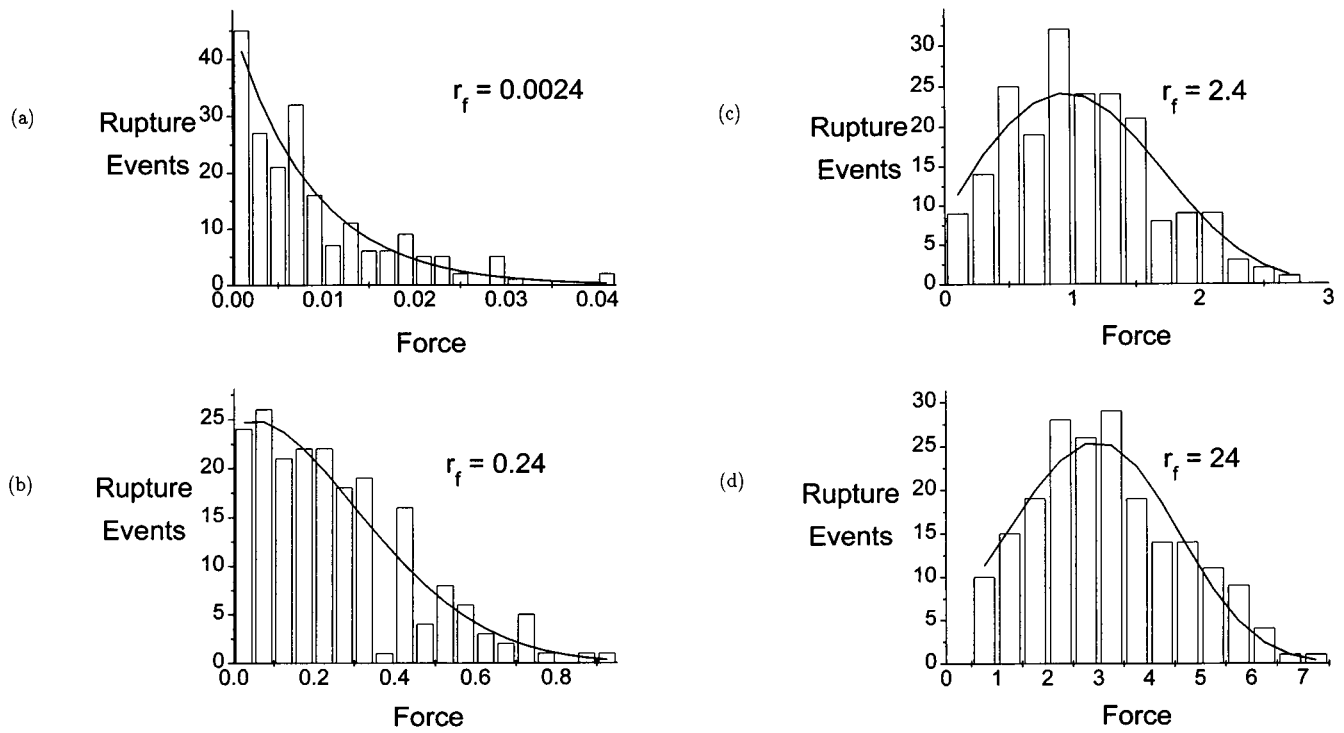

FIGURE 4 Histograms of rupture forces determined from 200 SMC simulations of bond breakage at widely separated loading rates. Superposed are optimal fits of the generic form of the probability distribution based on theoretical prediction for the off rate under force.

proportion to the logarithm of the loading rate [$f^* \sim \ln(r_f)$]. Independent of damping models, this fast loading regime spanned many decades of loading rate. Finally, plotted on a linear scale of loading rate in Figs. 6 *C* and 7 *C*, there was crossover to an ultrafast regime when $r_f > \sim\exp(E_b)$. On this scale, forces quickly overwhelmed the energy barrier. The regimes of strength at lower loading rates collapsed into the vertical axis so that bond strength seemed to emanate from a threshold at zero rate of loading. For the inverse power law attraction, strength leveled off above the threshold near the bare bond strength f_∞, which correlated with the value of E_b as expected from divergence of the off rate. But with the deep harmonic well, strength continued to rise weakly in proportion to the square root of the loading rate for $f > f_\infty(1 - 1/E_b^{1/2})$, retarded by transient outflow of states from the initial minimum. Endemic to all types of simulations, the continued rise in strength resulted from the rupture criterion defined as the final passage of a fixed position. Once forces overwhelm the bonding potential, all states are unbound, and only the naked viscous friction of the components is left to resist faster separation.

Last, we performed simulations of bond rupture in three dimensions for two spherical particles held in an inverse power law potential. Comparison of the results plotted in Fig. 8 with Fig. 6 shows that simulations of bond breakage in 3-D simulations gave nearly identical bond strengths to those obtained in 1-D simulations except at very slow loading rates. Under rates that led to large forces, it is not surprising that 3-D kinetics look like 1-D kinetics, because the reaction pathway is strongly collimated by force, and unbonding is favored in one direction. By comparison, under low rates and small forces, the reaction coordinate becomes delocalized in 3-D simulations with many pathways for unbonding that have nearly equivalent energy contours. For spherically symmetric potentials and weak forces, these trajectories are distributed almost uniformly over polar angle θ relative to the direction of force. Interestingly, for strong hydrodynamic interaction, the radial gradient in molecular mobility contributes a bias to the diffusive process analogous to a spherically symmetric force $\sim \nabla_r[\ln(D)]$, which significantly stimulates unbinding at weak forces. As noted earlier, strong hydrodynamic interaction in the absence of force has the effect of increasing the spatial dimension, which is consistent with the increases found in critical loading rates for both 1-D and 3-D simulations.

Rupture of biotin-avidin bonds in MD simulations

Unlike the idealized potentials treated earlier, energy landscapes of cell adhesion bonds and interfacial linkages involve interactions between many molecular groups. An example is the high affinity biotin-avidin complex bound together by several hydrogen bonds. Recently modeled in atomic detail, MD simulations were developed to determine the strength of biotin-streptavidin (Grubmuller et al., 1996) and biotin-avidin (Izrailev et al., 1997) bonds. In both

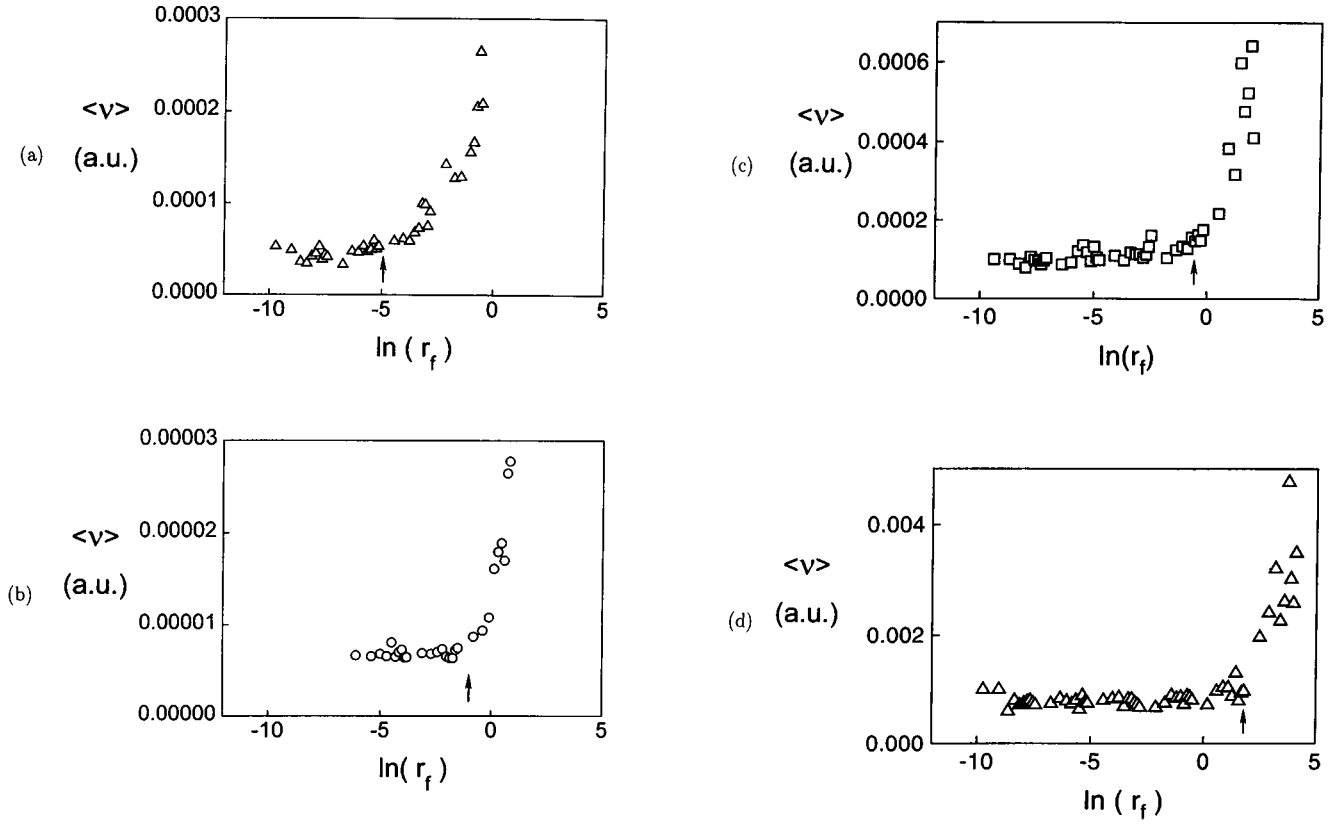

FIGURE 5 Apparent mean off rates (*a.u.*, arbitrary units) obtained from the decay in rupture events with rupture time demonstrate crossovers between spontaneous dissociation and force-driven kinetics at slow loading rates. Results for 1-D simulations assuming strong hydrodynamic interaction are plotted in (*A*) for inverse power law attraction and in (*B*) for a deep harmonic well. Results for 3-D simulations with inverse power law attraction are plotted in (*C*) for constant damping and in (*D*) for strong hydrodynamic interaction. The arrows mark the crossovers used to define the critical loading rates, r_f^c, and to derive empirical values for intrinsic repulsion, f_i.

simulations, biotin was extracted from the binding pocket by pulling on the outer end with a mechanical "spring," but the spring properties were quite different in each case. To estimate an energy landscape appropriate for the kinetics of unbonding in laboratory probe tests, we will use results from the simulation of Izrailev et al. (1997) kindly provided to us by Prof. Klaus Schulten and his group (Beckman Institute, University of Illinois). In their simulation, a highly extended spring was attached to biotin, and the spring stiffness, k_s, was increased from zero at a constant rate, $k_s = c_s t$. Because the magnitude of k_s stayed low over the course of detachment, fluctuations in spring force were small in comparison with the mean level of force, which increased steadily with time. Also, local diffusion was restricted minimally by the spring and allowed a good sample over local fast degrees of freedom at the slowest force-driven detachment, as shown by the profile of instantaneous energies in Fig. 9 *A*. Here, we consider only the sequence of interactions obtained when biotin was inside the binding pocket, which represented a range of mean separation up to ~1.3 nm. Even though biotin is pulled out of the binding pocket at speeds of ~1 nm/ns (= 1 m/s), the fluctuations in biotin velocity remain Maxwellian, with a mean square value of ~12,000 m^2/s^2, which exhibits a rapidly decaying correlation in time. Ideally, if separated slow enough, local averages over the enormous fluctuations in potential should yield a smooth potential $\langle E \rangle = E(x)$, where the mean force $f(x)$ sensed by the spring would equal $\partial E/\partial x$, and the local mean square fluctuation in position would reflect the curvature of the smooth potential plus the spring stiffness, i.e., $\langle \delta x^2 \rangle = k_B T/(\partial^2 E/\partial x^2 + k_s)$. Optimizing the averaging window ($\Delta t \sim 20$ ps), the outcome of this coarse-graining procedure is shown in Fig. 9 *B* along with a smooth polynomial approximation that closely fits the averaged potential. In regions dense with many local states, derivatives of the smooth polynomial are consistent with the values of mean spring force observed in the simulation and the mean square positional fluctuation calculated from the local distribution of states within an averaging window. However, easily recognized in Fig. 9 *A*, regions with few states represented outward jumps in position, the most prominent of which occurred between 0.4 and 0.8 nm. Over each jump region, the form of the smooth potential had to be approximated by analytic continuation with a cubic polynomial. (To achieve better statistics in these regions, the spring constant would have to be increased locally, and then the mean field could by derived from the logarithm of the distribution, taking proper account of the spring potential.)

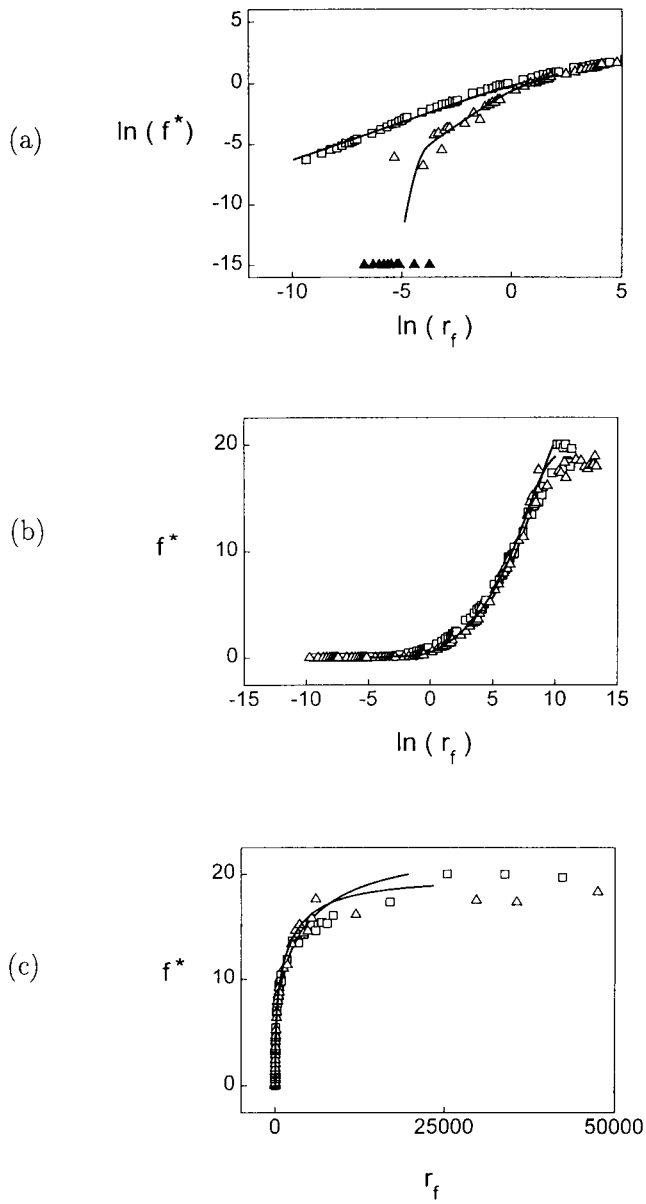

FIGURE 6 Strengths of bonds determined at fixed loading rates in 1-D simulations for an inverse power law potential (exponent $n = 4$) with a depth of $E_b = 5$. A comparison of viscous damping models is presented; the open triangles are results for strong hydrodynamic interaction, and open squares are results for constant damping. The curves are theoretical predictions for bond strength. (*A*) $\log(f^*)$ versus $\log(r_f)$ shows that strength emerges at a critical rate set by $f_i \approx 0.003$ for strong hydrodynamic interaction but seems to begin at zero rate for constant damping (*closed symbols* along the rate axis signify zero strength); (*B*) f^* versus $\log(r_f)$ shows crossover to the fast loading regime; (*C*) f^* versus r_f shows crossover to the ultrafast loading regime and the apparent threshold at zero loading rate.

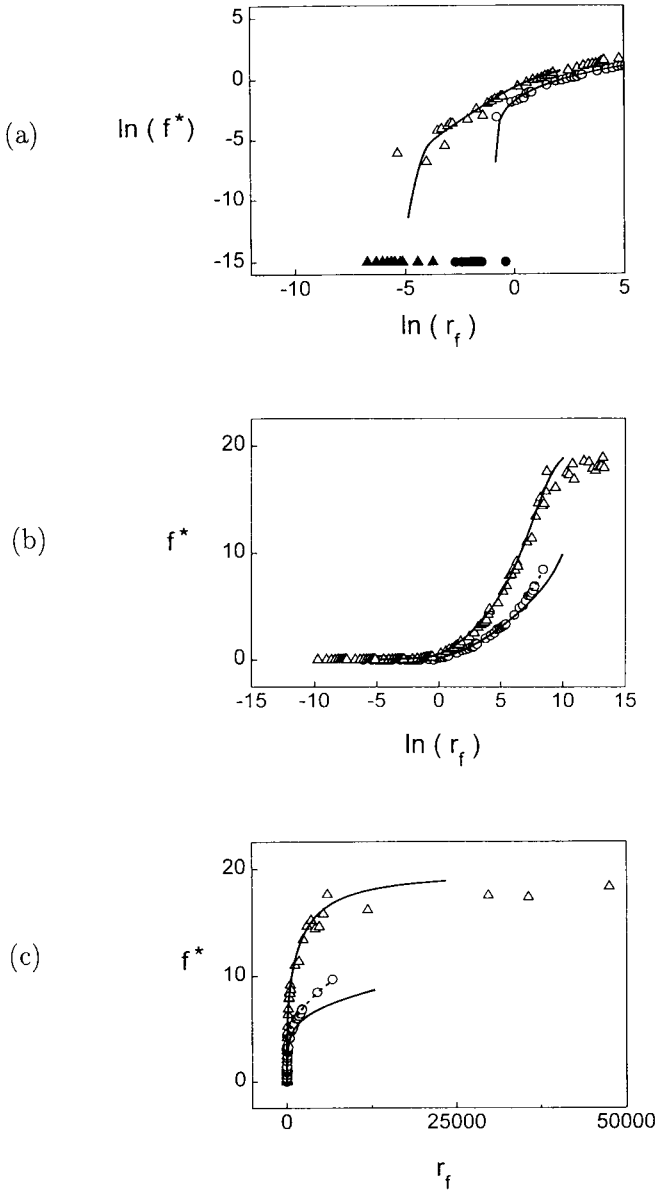

FIGURE 7 Strengths of bonds determined at fixed loading rates in 1-D simulations assuming strong hydrodynamic interaction. A comparison of bonding potentials is presented; open triangles are results taken from Fig. 6 for an inverse power law potential (exponent $n = 4$), and open circles are results for a deep harmonic well, both specified with a depth of $E_b = 5$. The curves are theoretical predictions for bond strength. (*A*) $\log(f^*)$ versus $\log(r_f)$ shows that strength emerges at critical rates set by $f_i \approx 0.003$ for the inverse power law attraction and $f_i \approx 0.18$ for the harmonic well (*closed symbols* along the rate axis signify zero strength); (*B*) f^* versus $\log(r_f)$ shows crossover to the fast loading regime; (*C*) f^* versus r_f shows crossover to the ultrafast loading regime and the apparent threshold at zero loading rate.

As shown by the relation for $\langle \delta x^2 \rangle$, the curvature of the averaged potential became negative in this region, and fluctuations were locally unconfined when $\partial^2 E/\partial x^2 < -k_s$. These jumps revealed inner transition states along the dissociation pathway. Applying an external force to the averaged potential, as shown in Fig. 10 *A*, we see that the energy barrier switches from the initial transition state at ~1.3 nm to the inner transition state at ~0.6 nm once forces exceed a mere 60 pN. Next, in Fig. 10 *B*, forces of ~280 pN lower the energy barrier to the level of the initial minimum, which would allow unencumbered diffusion past the barrier. Based on the value of intrinsic friction $\gamma_o \sim 2 \times 10^{-11}$ Ns/m

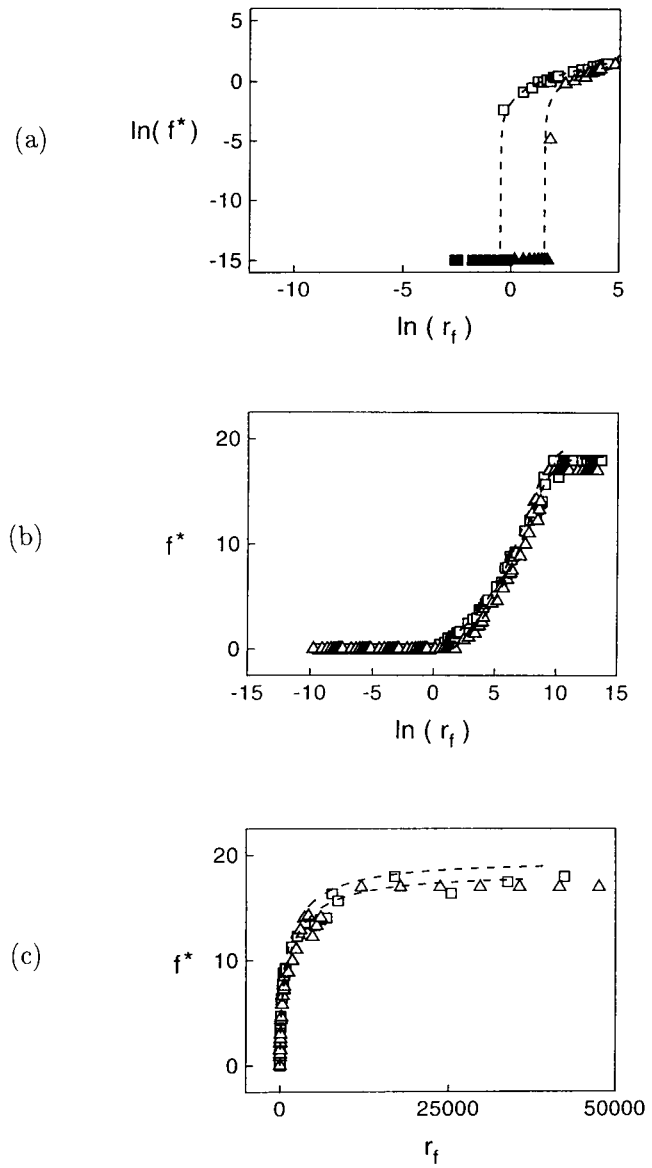

FIGURE 8 Strengths of bonds determined at fixed loading rates in 3-D simulations for an inverse power law potential (exponent $n = 4$) with a depth of $E_b = 5$. A comparison of viscous damping models in 3-D simulations is presented; open triangles are results for strong hydrodynamic interaction, and open squares are results for constant damping. The curves (*dashed*) are predictions of 1-D theory calculated using the empirical values of intrinsic repulsion derived from the critical loading rates in Fig. 5 *C* and *D*. (*A*) $\log(f^*)$ versus $\log(r_f)$ shows that strength emerges at critical rates set by $f_i \approx 1.5$ for strong hydrodynamic interaction and by $f_i \approx 0.32$ for constant damping (*closed symbols* along the rate axis signify zero strength); (*B*) f^* versus $\log(r_f)$ shows crossover to the fast loading regime; (*C*) f^* versus r_f shows crossover to the ultrafast loading regime and the apparent threshold at zero loading rate.

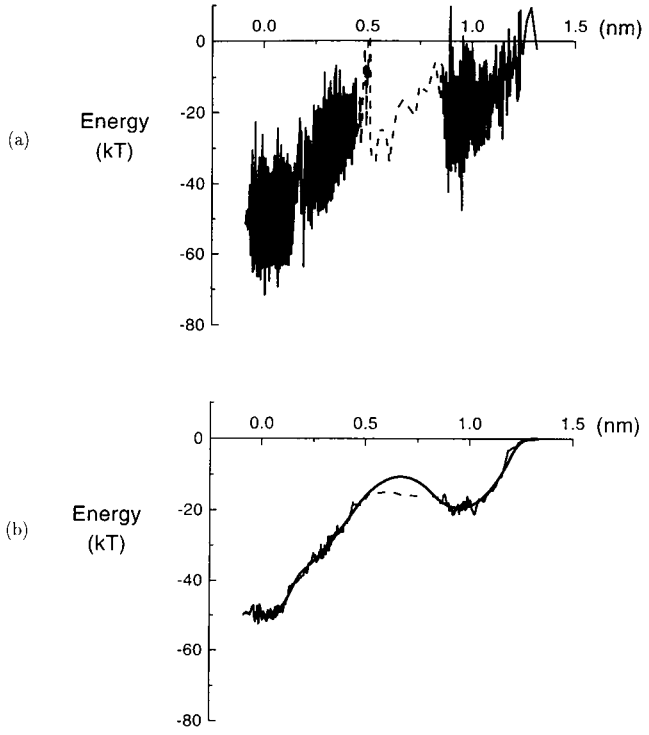

FIGURE 9 Derivation of an approximate energy landscape for force-driven dissociation of biotin-avidin bonds. (*A*) Instantaneous energies computed along the detachment path in the slowest simulation (~500 ps) of Izrailev et al. (1997) (kindly provided to us by Professor Klaus Schulten and co-workers, Beckman Institute, University of Illinois). (*B*) Coarse-grained average of the instantaneous energies (*thin curve*) and the smooth polynomial fit used to estimate of the potential of mean force (*thick curve*). Dashed segments in the thin curve represent jumps with few statistics. Over these jumps, the smooth potential was connected by analytic continuation with a cubic polynomial.

implied by the simulation of Grubmuller et al. (1996), we can estimate the characteristic time for diffusive passage of the transition state. Recalling that $t_D = x_a x_{ts}/(k_B T/\gamma_o) \sim 0.1$ nm^2/(2×10^8 nm^2/s), $t_D \sim 500$ ps would represent the expected lifetime of the bond under a constant external force of 280 pN. However, if the rate of loading is $> 280/t_D \sim 10^{12}$ pN/s, then the bond would remain kinetically trapped, and force would continue to rise. Finally, in Fig. 10*C*, forces of > 400 pN completely eliminate the barrier as set by the maximum gradient in the coarse-grained potential. For the slowest detachment in the simulation of Izrailev et al. (1997), the loading rate was almost constant at $\sim 1.3 \times 10^{12}$ pN/s and led to a rupture force of ~450 pN after about 350 ps, which is consistent with the maximum potential gradient.

In contrast to the simulation by Izrailev et al. (1997), biotin was pulled from a streptavidin-binding pocket with a very stiff zero-length spring, moved at constant speed, in the simulation by Grubmuller et al. (1996). Because the value of the spring constant was large ($k_s = 2800$ pN/nm), the spring force fluctuated strongly as biotin was forced to jump from one local region of molecular attraction to the next during separation. Because of the frequent jumps, biotin moved almost steadily out of the binding pocket, and the pulling force appeared to be augmented by a viscous drag proportional to the speed of separation, which provided the estimate of $\sim 2 \times 10^{-11}$ Ns/m for intrinsic friction. At the slowest pulling speed, ~1.5 m/s, the maximum force along the path was ~300 pN (when averaged over a few ps),

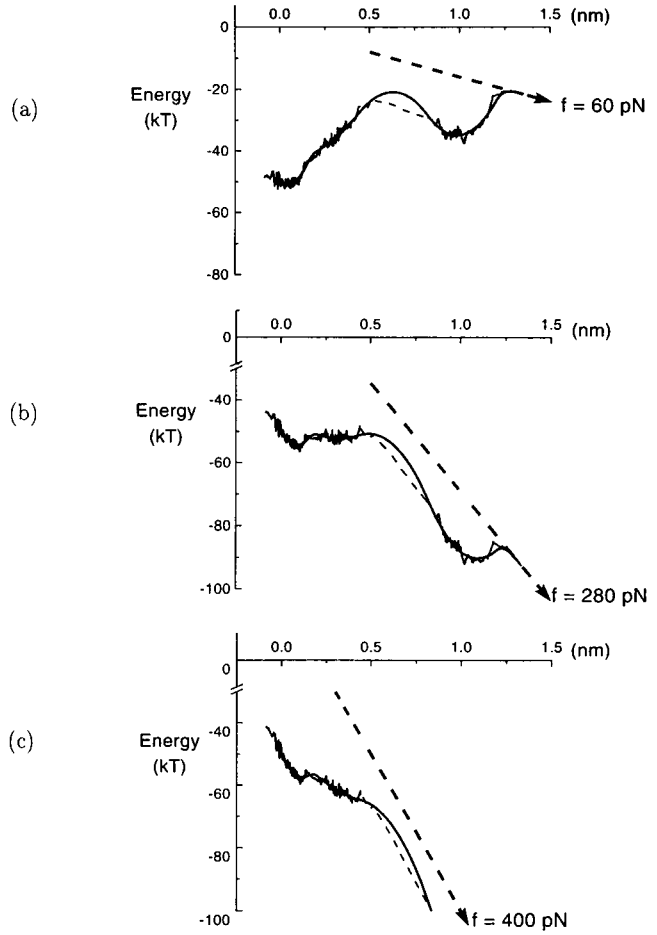

FIGURE 10 Tilt of the smooth energy landscape in Fig. 9 *B* by external force. (*A*) For forces ≥60 pN, the transition state shifts inward from the outer barrier at ~1.3 nm to the inner barrier at ~0.6 nm. (*B*) Forces of ~280 pN lower the barrier to the level of the initial energy minimum, which would allow free diffusion past the barrier for states starting at the initial minimum. (*C*) When forces reach the level (~400 pN) of the maximum gradient in the coarse-grained potential, all barriers are eliminated, and the potential is completely overwhelmed by the applied force.

considerably less than for the slowest simulation of Izrailev et al. (1997). The lower value of rupture force could have been the consequence of convection of biotin through local minima by the stiff-moving spring. As such, the characteristic time needed for diffusion past local barriers would have been greatly reduced to ~8 ps based on the spring stiffness (i.e., $k_BT/k_s \sim (0.04\ \text{nm})^2$]. Thus, the mean spring force would continue to rise above the local threshold strength for about 8 ps, and the added force would be proportional to the spring loading rate ($k_s \times$ speed), which is consistent with the results of Grubmuller et al. (1996) for speeds slower than 10 m/s. Above 15 m/s, rupture forces became erratic, perhaps because of insufficient time for local thermal equilibration.

With the value of intrinsic friction and the coarse-grained potential, we have used the theoretical approach developed earlier to derive the full spectrum of strength for steady rates of loading below 10^{12} pN/s. These estimates are not to be taken as accurate predictions but only serve to illustrate how to bridge the enormous gap in time scales between MD simulations and laboratory measurements. Plotted in Fig. 11, the calculations of strength show separate regimes of logarithmic dependence on loading rate, $f^* \sim (k_BT/x_{ts})\ \ln(\Delta f/\Delta t)$ + const, where the break in slope results from the switch in transition state from x_{ts} of ~1.3 to ~0.6 nm at forces above ~60 pN. Above 280 pN, there is crossover to the ultrafast regime, in which drift kinetics lead to $f^* \sim (f_{\infty'}t_D \cdot \Delta f/\Delta t)^{1/2}$ with $f_{\infty'}$ = 280 pN. Superposed on the calculated strengths in Fig. 11 are the ranges of force that would be sensed by different force probe techniques. The range for each technique is based on nominal loading rates (i.e., the fastest loading rates, ~10^4–10^5 pN/s, for the AFM; intermediate loading rates, ~10–10^3 pN/s, for the BFP; and the slowest loading rates, ~1–10 pN/s, for the OT). The label MD notes the rupture force determined at the slowest rate of loading, ~1.3 × 10^{12} pN/s, in the simulation of Izrailev et al. (1997). As shown by the labels, the force estimates for laboratory probes are governed by the inner transition state except perhaps under very slow rates, <1

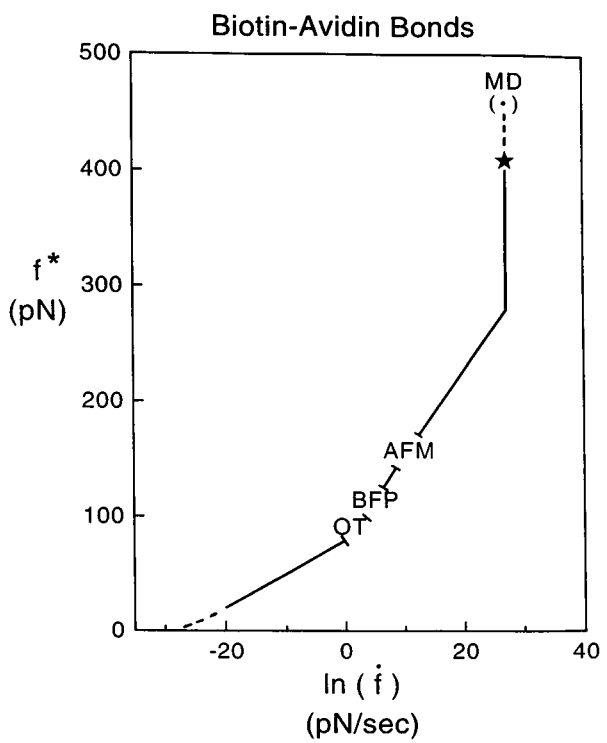

FIGURE 11 Hypothetical strengths of biotin-avidin bonds calculated over 12 orders of magnitude in loading rate using the energy landscape shown in Fig. 9 *B*. The estimates of bond strength are plotted versus the logarithm of loading rate (ln(pN/s)). Breaks in the plot indicate the range of rupture forces expected for different laboratory probe techniques based on loading rates: i.e., the AFM for the fastest loading rates, ~10^4–10^5 pN/s; the BFP for intermediate loading rates, ~10–10^3 pN/s; and the OT for the slowest loading rates. ~1–10 pN/s. The maximum strength predicted by the coarse-grained potential is noted by the star. Also, the label MD represents the rupture force determined under the slowest rate of loading, ~10^{12} pN/s, in the simulation of Izrailev et al. (1997).

pN/s, but estimates for each technique yield a different range of strengths.

CONCLUSIONS

Applied to situations of constant loading rate, Kramers' Brownian dynamics theory predicts three generic regimes of bond strength. These predictions have been confirmed by SMC simulations of idealized bonds loaded under a ramp of force in an overdamped environment (liquids). The power of Kramers' theory is demonstrated by the accuracy of the predictions over the full range of strength, including subtle effects of models for molecular mobility and sensitivity to details of the potentials, i.e., constant damping vis à vis separation-dependent damping, steepness of the potential and specific exponents, etc. The theory and simulations reveal the inherent dynamic nature of bond strength, which provides important insights into how forces can be expected to vary in tests of the same bonds with different types of laboratory probes and how laboratory measurements can be related to detailed molecular-scale simulations in MD.

Most relevant to biology, low strengths arise in a slow loading regime that depends on how small forces deform the bonding potential and initially shape the transition state in the region of very weak attraction. For purely attractive potentials that vanish monotonically at large distances, a traditional challenge has been how to overcome the pathological feature of Kramers' theory in one dimension, in which no spontaneous dissociation is predicted in the absence of external force. As a possible rationalization, we have postulated that crossover from force-driven kinetics to spontaneous dissociation can be introduced empirically by simply defining a small intrinsic repulsion. As such, bond strength begins once the loading rate is sufficient to produce forces above the inherent repulsion on the time scale of spontaneous dissociation. Here, simulations have provided crucial tests of a crossover to spontaneous dissociation and the critical rate hypothesis. But as shown earlier, identification of a critical loading rate is nontrivial and depends on the model of molecular damping, the type of bonding potential, and spatial dimensionality. For strong hydrodynamic interaction in which damping diminishes with separation at close range, nonzero critical rates were found in all simulations. Significantly, the value of intrinsic repulsion derived from the observed critical rates increased by 300-fold between 1-D and 3-D simulations, which implies that curvature of a bonding surface affects the crossover from spontaneous to force-driven dissociation for large molecular complexes. Although a critical rate of loading was found in simulations with strong hydrodynamic interaction, no critical rate could be established in 1-D simulations with constant damping even at the most lethargic rate, at which bond strength dropped to less than 1/1000 of the thermal force scale. This result does not rule out the existence of a critical loading rate for constant damping in 1-D simulations but merely sets an upper bound. On the other hand, at higher rates of loading, the bond strengths measured in 1-D and 3-D simulations were indistinguishable for both models of viscous damping. In this less intriguing fast regime, bond strength rises essentially as the logarithm of the loading rate over an enormous span in loading rate determined by the reciprocal of the Arrhenius factor. The logarithmic dependence stems from the exponential amplification in the likelihood of reaching the top of the energy barrier as force rises above the characteristic thermal force. Ultimately, at extreme rates of loading, an ephemeral ultrafast regime is entered in which the mechanical potential quickly overwhelms the most prominent energy barrier along the reaction pathway, leaving all states free to unbind.

It is clear that strengths of molecular linkages must be tested under controlled loading over a wide range of rates. When applied this way, probe techniques can be used as a dynamic force spectroscopy to reveal prominent features of the energy landscape along a force-driven pathway to rupture. With cautious respect for inherent uncertainties, measurements on laboratory time scales can be compared with predictions of MD simulations on extremely fast time scales using Brownian dynamics simulations. Derived from averages over the nanosecond time frame set by current MD computations, the potential of mean force and frictional damping along the selected reaction coordinate should be coupled with a collective mechanical model of the slow configurational excitations to provide the best Brownian dynamics abstraction. As shown by the simple analysis of biotin-avidin results (Izrailev et al., 1997) in the previous section, rupture forces derived from MD simulations can significantly exceed levels expected for force probe measurements, and there is no a priori reason to correlate laboratory tests of bond strength with the apparent threshold seen in MD. The apparent threshold should be merely viewed as the level of force sufficient to eliminate kinetic barriers to unbonding and predicts only an upper bound for forces in probe measurements.

We thank Dr. David Boal (Simon Fraser University) for his help in setting up a Metropolis Monte Carlo algorithm, the computer graphics for imaging simulations, and many important discussions. Also, we appreciate the help of Mr. Mike Minton, who ran many of the initial simulations as part of his undergraduate honors physics thesis. Special thanks go to Prof. Klaus Schulten and co-workers (Beckman Institute, University of Illinois) for sharing results and discussing important details of their biotin-avidin simulation before publication.

This work was supported by grants HL 54700 and HL 31579 from the National Institutes of Health and grant OGP 155415 from the National Science and Engineering Research Council of Canada.

REFERENCES

Alon, R., D. A. Hammer, and T. A. Springer. 1995. Lifetime of the P-selectin-carbohydrate bond and its response to tensile force in hydrodynamic flow. *Nature.* 374:539–542.

Ansari, A., C. M. Jones, E. R. Henry, J. Hofrichter, and W. A. Eaton. 1992. The role of solvent viscosity in the dynamics of protein conformational changes. *Science.* 256:1796–1798.

Ansari, A., C. M. Jones, E. R. Henry, J. Hofrichter, and W. A. Eaton. 1994. Conformational relaxation and ligand binding in myoglobin. *Biochemistry.* 33:5128–5145.

Ashkin, A., K. Schutze, J. M. Dziedzic, U. Euteneuer, and M. Schliwa. 1990. Force generation of organelle transport measured in vivo by an infrared laser trap. *Nature.* 348:346–348.

Batchelor, G. K. 1976. Brownian diffusion of particles with hydrodynamic interaction. *J. Fluid Mech.* 74:1–29.

Bell, G. I. 1978. Models for the specific adhesion of cells to cells. *Science.* 200:618–627.

Dembo, M., D. C. Torney, K. Saxman, and D. Hammer. 1988. The reaction limited kinetics of membrane to surface adhesion and detachment. *Proc. R. Soc. Lond. B. Biol. Sci.* 234:55–83.

Evans, E. 1995. Physical actions in biological adhesion. *In* Structure and Dynamics of Membranes. Handbook of Physics of Biological Systems, Vol 1. R. Lipowsky and E. Sackmann, editors. Elsevier Science BV, Amsterdam. 723–754.

Evans, E., D. Berk, and A. Leung. 1991. Detachment of agglutinin bonded red blood cells: I. Forces to rupture molecular-point attachments. *Biophys. J.* 59:838–848.

Evans, E., R. Merkel, K. Ritchie, S. Tha, and A. Zilker. 1994. Picoforce method to probe submicroscopic actions in biomembrane adhesion. *In* Studying Cell Adhesion. P. Bongrand, P. M. Claesson, and A. S. G. Curtis, editors. Springer-Verlag, Berlin. 125–140.

Evans, E., K. Ritchie, and R. Merkel. 1995. Sensitive force technique to probe molecular adhesion and structural linkages at biological interfaces. *Biophys. J.* 68:2580–2587.

Florin, E.-L., V. T. Moy, and H. E. Gaub. 1994. Adhesive forces between individual ligand-receptor pairs. *Science.* 264:415–417.

Green, N. M. 1975. Avidin. *Adv. Protein Chem.* 29:85–133.

Grubmuller, H., B. Heymann, and P. Tavan. 1996. Ligand binding: molecular mechanics calculation of the streptavidin-biotin rupture force. *Science.* 271:997–999.

Hanggi, P., P. Talkner, and M. Borkovec. 1990. Reaction-rate theory: fifty years after Kramers. *Rev. Mod. Phys.* 62:251–342.

Hoh, J. H., J. P. Cleveland, C. B. Prater, J.-P. Revel, and P. K. Hansma. 1992. Quantized adhesion detected with the atomic force microscope. *J. Am. Chem. Soc.* 114:4917–4918.

Izrailev, S., S. Stepaniants, M. Balsera, Y. Oono, and K. Schulten. 1997. Molecular dynamics study of unbinding of the avidin-biotin complex. *Biophys. J.* 72:1568–1581.

Kramers, H. A. 1940. Brownian motion in a field of force and the diffusion model of chemical reactions. *Physica (Utrecht).* 7:284–304.

Kuo, S. C., and M. P. Sheetz. 1993. Force of single kinesin molecules measured with optical tweezers. *Science.* 260:232–234.

Lee, G. U., D. A. Kidwell, and R. J. Colton. 1994. Sensing discrete streptavidin-biotin interactions with atomic force microscopy. *Langmuir.* 10:354–357.

Metropolis, N., A. W. Rosenbluth, M. N. Rosenbluth, A. H. Teller, and E. Teller. 1953. Equation of state calculations by fast computing machines. *J. Chem. Phys.* 21:1087–1092.

Moy, V. T., E.-L. Florin, and H. E. Gaub. 1994. Intermolecular forces and energies between ligands and receptors. *Science.* 266:257–259.

Radmacher, M., R. W. Tillmann, M. Fritz, and H. E. Gaub. 1992. From molecules to cells: imaging soft samples with the atomic force microscope. *Science.* 257:1900–1905.

Rossky, P. J., J. D. Doll, and H. L. Friedman. 1978. Brownian dynamics as smart Monte Carlo simulation. *J. Chem. Phys.* 69:4628–4633.

Tees, D. F. J., O. Coenen, and H. L. Goldsmith. 1993. Interaction forces between red cells agglutinated by antibody. IV. Time and force dependence of break-up. *Biophys. J.* 65:1318–1334.

Williams, J. M., T. Han, and T. P. Beebe, Jr. 1996. Determination of single-bond forces from contact force variances in atomic force microscopy. *Langmuir.* 12:1291–1295.